Nano Research

ISSN 1998-0124 CN 11-5974/O4
https://doi.org/10.1007/s12274-018-2193-7

Research Article

Quasi-two-dimensional β-Ga_2O_3 field effect transistors with large drain current density and low contact resistance via controlled formation of interfacial oxygen vacancies

Zhen Li[§], Yihang Liu[§], Anyi Zhang, Qingzhou Liu, Chenfei Shen, Fanqi Wu, Chi Xu, Mingrui Chen, Hongyu Fu, and Chongwu Zhou (✉)

Ming Hsieh Department of Electrical Engineering, Mork Family Department of Chemical Engineering and Material Science, Department of Physics and Astronomy, University of Southern California, Los Angeles, California, 90089, USA
[§] *Zhen Li and Yihang Liu contributed equally to this work.*

Received: 3 June 2018 / **Revised:** 31 August 2018 / **Accepted:** 5 September 2018

ABSTRACT

Quasi-two-dimensional (2D) β-Ga_2O_3 is a rediscovered metal-oxide semiconductor with an ultra-wide bandgap of 4.6–4.9 eV. It has been reported to be a promising material for next-generation power and radio frequency electronics. Field effect transistors (FETs) that can switch at high voltage are key components in power and radio frequency devices, and reliable Ohmic contacts are essential for high FET performance. However, obtaining low contact resistance on β-Ga_2O_3 FETs is difficult since reactions between β-Ga_2O_3 and metal contacts are not fully understood. Herein, we experimentally demonstrate the importance of reactions at the metal/β-Ga_2O_3 interface and the corresponding effects of these reactions on FET performance. When Ti is employed as the metal contact, annealing of β-Ga_2O_3 FETs in argon can effectively transform Schottky contacts into Ohmic contacts and permit a large drain current density of ~ 3.1 mA/μm. The contact resistance ($R_{contact}$) between the Ti electrodes and β-Ga_2O_3 decreased from ~ 430 to ~ 0.387 Ω·mm after annealing. X-ray photoelectron spectroscopy (XPS) confirmed the formation of oxygen vacancies at the Ti/β-Ga_2O_3 interface after annealing, which is believed to cause the improved FET performance. The results of this study pave the way for greater application of β-Ga_2O_3 in electronics.

KEYWORDS

quasi-two-dimensional material, metal-oxides, field effect transistor, β-Ga_2O_3, contact resistance

1 Introduction

β-Ga_2O_3 was recently unveiled as a promising wide bandgap quasi-two-dimensional (2D) semiconducting material with interesting optical and electrical properties [1–10]. Advancements in bulk single crystal β-Ga_2O_3 growth methods and β-Ga_2O_3-based field-effect transistors (FETs) have attracted much attention in this regard and ignited substantial scientific interest [6, 7, 11]. β-Ga_2O_3 is not strictly a 2D material. However, owing to the large lattice constant of 12.33 Å along the [100] direction in a monoclinic β-Ga_2O_3 crystal [7, 8], quasi-2D β-Ga_2O_3 nanomembranes can be mechanically exfoliated from cleavage planes of a β-Ga_2O_3 crystal, similar to exfoliation of 2D materials [7–15]. Previously, Hwang et al. obtained 20 nm β-Ga_2O_3 nanomembranes after exfoliation [6]. Zhou et al. reported that the threshold voltage would shift from negative values in depletion mode to positive values in enhance mode by reducing the thickness of β-Ga_2O_3 nanomembranes from 100 to 50 nm, but the drain current would also significantly decrease [9]. Large on-state currents [7, 9, 16], high breakdown voltage [17, 18], excellent on/off ratios [7, 9, 17], and the potential of operating in radio frequency regime [19] have been reported in FETs based on exfoliated β-Ga_2O_3. Although β-Ga_2O_3 is a competitive candidate for use in next-generation electronics [6, 7, 17], FETs made with β-Ga_2O_3 usually exhibit significant Schottky barriers [6, 7, 20–22], resulting in high contact resistance and small on-state current, thus hampering FET performance [23–26]. For semiconducting metal-oxides, metal contacts often react with metal-oxides at the interface to produce complex compounds, making the problem even more complicated [27–34]. Unfortunately, these reactions involving β-Ga_2O_3 have not been well documented, leaving a gap in the collective understanding of interfacial reactions and their corresponding effects on the electronic properties of β-Ga_2O_3 devices [21, 35]. Hence, to fully develop the potential of β-Ga_2O_3, reliable Ohmic contacts and an investigation of reactions at metal/β-Ga_2O_3 interface are required.

Several methods have been used to improve electrical contacts at the metal/semiconductor interface, such as gas adsorption, doping techniques, and exploiting interfacial reactions [4, 23–26, 36–41]. Even though metal/β-Ga_2O_3 contacts have not been thoroughly studied, significant research has focused on some other metal-oxides, such as titanium dioxide (TiO_2) and indium oxide (In_2O_3) [26–33, 40–44], which can provide insight on improving metal/β-Ga_2O_3 contacts. As a well-known metal-oxide, TiO_2 can be readily reduced by most electrode metals [27–34, 42, 43]. Furthermore, by comparing the electronic performance of TiO_2-based memristors with different contact metals, it was shown that oxygen vacancies created by reactions at metal/TiO_2 interfaces dominate other factors in determining the device performance [27–34, 43]. Previously, we reported that In_2O_3 nanowire FETs exhibited a pronounced increase in conductance after baking in vacuum [44, 45]. In contrast, baking the FETs in ambient air led to a reduction in carrier concentration and caused

Address correspondence to chongwuz@usc.edu

drastic suppression in device performance [44]. The underlying mechanism is that baking In_2O_3 nanowire FETs in vacuum led to oxygen vacancy formation in In_2O_3, resulting in increased dopant concentration and higher conductance [44]. On the other hand, baking In_2O_3 nanowire FETs in air led to reduced oxygen vacancy concentration, lower n-type doping, and hence lower conductance [43, 44]. The above phenomena allow us to tune the Schottky barriers formed between the metal contacts and β-Ga_2O_3, which would improve the efficiency of charge injection at the metal/β-Ga_2O_3 interface and lower the contact resistance [27–34, 43–47].

Different dopants and contact materials were investigated to suppress the contact resistance in n-type and p-type β-Ga_2O_3 FETs [7, 20, 48]. N-type devices with indium tin oxide (ITO) or aluminum zinc oxide (AZO) contacts exhibited low contact resistance of ~ 0.5–0.6 Ω·mm [49, 50]. Meanwhile, argon plasma bombardment has been used to produce a large on-state current density of ~ 0.65 mA/μm, but no current saturation was observed [9, 16]. P-type β-Ga_2O_3 FETs were also fabricated using Zn or Mg doping, but the hole mobility and on-state current of p-type β-Ga_2O_3 FETs was still undesirable [20, 51]. Until now, the effects of interactions between electrical contacts and β-Ga_2O_3 still require more investigation [15, 21–35]. Therefore, transfer line measurements (TLM) and X-ray photoelectron spectroscopy (XPS) are required to determine the contact resistance and systematically investigate interface reactions [23, 27, 46].

In this study, we report that n-type β-Ga_2O_3 FETs made with Ti/Au contacts could exhibit a large saturation drain current density of ~ 3.1 mA/μm and low contact resistance of ~ 0.387 Ω·mm after annealing in argon atmosphere. Here, we demonstrate that such a simple yet effective argon annealing process can significantly improve the performance of β-Ga_2O_3 FETs with Ti/Au contacts. Annealing causes the β-Ga_2O_3 FETs with Ti/Au contacts can be switched from Schottky to Ohmic behavior. More interestingly, annealing in argon led to the formation of oxygen vacancies at the Ti/β-Ga_2O_3 interface [27, 30–34, 43, 52], effectively reducing the Schottky barriers at the interface and providing reliable Ohmic contacts. All electronic measurements and XPS results suggest that annealing is a reliable and generic approach to improve the performance of β-Ga_2O_3 FETs.

2 Results and discussion

β-Ga_2O_3 was first exfoliated with vacuum tape, yielding membranes with thickness measuring tens of nanometers. After exfoliation, the nanomembranes were dry-transferred onto a Si wafer with silicon oxide (SiO_2) thickness of 300 nm. An atomic force microscopy (AFM) image of a typical β-Ga_2O_3 nanomembrane is shown in Fig. 1(a), revealing that the thickness of the nanomembrane is ~ 80 nm. High-resolution transmission electron microscopy (HRTEM) was used to further explore the structural properties of quasi-layered β-Ga_2O_3. The TEM image of a β-Ga_2O_3 nanomembrane is shown on the left part of Fig. 1(b). It clearly shows β-Ga_2O_3 (002) atomic planes with a lattice spacing of ~ 0.28 nm, which agrees well with other results in the literature [11, 12]. The right portion of Fig. 1(b) shows a fast Fourier transform (FFT) spectrum, revealing the lattice group symmetry and parameters [11, 12]. Raman spectroscopy was also used to investigate the quality of the exfoliated β-Ga_2O_3 nanomembranes (Fig. S1 in the Electronic Supplementary Material (ESM)). The phonon positions in the exfoliated nanomembranes are the same as those in bulk β-Ga_2O_3, indicating the structure of β-Ga_2O_3 nanomembranes did not degrade during mechanical exfoliation [52]. A schematic diagram of a typical β-Ga_2O_3 backgated FET is shown in Fig. 1(c). Heavily p-type doped Si was used as the common back gate, and the gate dielectric was a thermally grown 300 nm thick SiO_2 layer. Pure Ti/Au (10 nm/150 nm) contacts were defined using e-beam lithography followed by e-beam metal deposition under high vacuum to form the source and drain electrodes [26]. More experimental details on device fabrication can be found in the Methods section. Figure 1(d) shows an optical image of a β-Ga_2O_3 FET. Scanning electron microscopy (SEM) was used to capture images of the channel area. The inset SEM image in Fig. 1(d) shows the channel area in the β-Ga_2O_3 FET; the channel width is ~ 5.1 μm and the channel length is ~ 550 nm. Next, we studied the electronic performance of this β-Ga_2O_3 FET before and after annealing. Strong asymmetric Schottky behavior can be clearly observed from the nonlinear trend in the I_{ds}-V_{ds} curve before annealing (black curve), as shown in Fig. 1(e). The as-made β-Ga_2O_3 FET was annealed in a quartz tube that was flushed with pure argon to clear any residual gas species from the system. After annealing at 300 °C for 180 min, the Ohmic contact behavior of β-Ga_2O_3 FET was observed, as indicated by the red curve in Fig. 1(e). Surprisingly, the enhanced on-state drain current is 3 orders of magnitude larger than in the unannealed sample, suggesting that the electrical contacts on the β-Ga_2O_3 FET significantly improved after annealing in argon atmosphere. The improved device performance indicates a transition from Schottky to Ohmic contacts at the Ti/β-Ga_2O_3 interface, which also resulted in current saturation. Figure 1(f) shows the output characteristics of the as-made β-Ga_2O_3 FET. Drain current saturation in this device was observed when high drain voltage was applied. The device operated with increasing drain voltage, reaching a large drain current density of ~ 3.1 mA/μm at V_{ds} = 100 V. The Ohmic contacts enable outstanding performance that can survive at high voltages and switch under large drain currents without avalanche or ionization breakdown. Compared to other recent studies reporting the current density in β-Ga_2O_3 FETs [7, 9, 16], our result is the highest saturation drain current density reported to date. A comparison

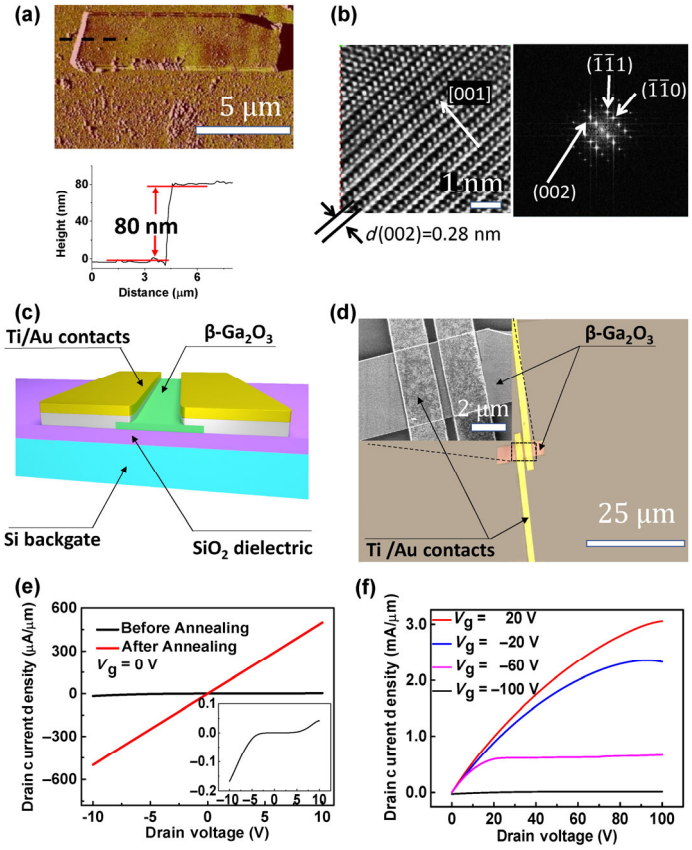

Figure 1 Characteristics of β-Ga_2O_3 and typical β-Ga_2O_3 FETs. (a) AFM image and height profile of a β-Ga_2O_3 flake. (b) TEM characterization of β-Ga_2O_3. (c) Scheme of a typical β-Ga_2O_3 FET with Ti/Au contacts. (d) Optical image of a β-Ga_2O_3 FET with Ti/Au contacts. The inset shows an SEM image of the channel area. (e) I_{ds}–V_{ds} curves from the β-Ga_2O_3 FET before (black curve) and after (red curve) annealing at 300 °C in argon. The inset image shows an enlarged I_{ds}–V_{ds} curve before annealing to illustrate the Schottky behavior. (f) I_{ds}–V_{ds} family curves from an annealed β-Ga_2O_3 FET under high V_{ds}.

between our results and other reported results can be found in Table S1 in the ESM. Considering their quasi-2D properties, β-Ga_2O_3 FETs can be easily integrated in various platforms for power and radio frequency electronics, which are desirable for microscale on-chip management applications. Moreover, the device performance remained nearly constant even after exposure to ambient air at room temperature for two months, which the air β-Ga_2O_3 FETs are stable in air (Fig. S2 in the ESM).

We systematically studied the effectiveness of argon annealing for improving the electronic performance of β-Ga_2O_3 FETs. The typical transfer characteristics (I_{ds}–V_g curves) in a β-Ga_2O_3 FET before and after annealing at 10, 30, 60, and 180 min are shown in Fig. 2(a). We found that annealing in argon at 300 °C for only 10 min can significantly increase the on-state current density. Figure 2(b) shows I_{ds}–V_g curves from this β-Ga_2O_3 FET in logarithmic scale. The on-state current density continued to increase when the FET was sequentially annealed and reached a maximum of ~ 620 μA/μm at V_{ds} = 12 V, which was almost 3,000 times larger than the drain current density before annealing. In addition, one can clearly see that the device showed a low off-state current density of ~ 10^{-7} μA/μm even after annealing in argon for 180 min, resulting in a very high on/off ratio of ~ 6×10^9. Output characteristics of the β-Ga_2O_3 FET are shown in Figs. 2(c) and 2(d). The I_{ds}-V_{ds} family curves from the β-Ga_2O_3 FET before annealing are shown in Fig. 2(c), where nonlinear behavior can be observed at small V_{ds} values. A strong Schottky barrier with a rather small drain current density ~ 0.18 μA/μm at V_{ds} = 12 V can be observed in the device. After annealing in argon for 180 min, Ohmic contact behavior in this device can be seen from Fig. 2(d). The substantially improved device performance after annealing shows that high temperature treatment can transform the Schottky contacts between Ti and β-Ga_2O_3 into Ohmic contacts. It is also worth mentioning that the improvements after annealing are highly reproducible. We fabricated multiple β-Ga_2O_3 FETs to test their performance and examine the generality of annealing for improving the device performance. Statistics of the key figures of merit are shown in Figs. 2(e) and 2(f). Significantly improved FET performance was observed after annealing in all devices. All devices showed substantially increased on-state current density at different annealing times. In Fig. 2(e), we note that all the devices show a large on-state current of several hundred microamperes after annealing for 180 min. Similar improvement of field effect mobility after annealing in argon can also be seen from Fig. 2(f). These effective mobility values were estimated using the standard FET model (See Methods for more details). Again, the β-Ga_2O_3 FET after annealing exhibits much higher mobility. The maximum field-effect mobility reaches ~ 65 $cm^2/(V{\cdot}s)$ after annealing the device in argon for 180 min. Such large on-state current, high on/off ratio, and electron mobility offer the promise of using β-Ga_2O_3 in power electronic devices and radio frequency applications. Furthermore, we noticed that annealing the devices at higher temperature (500 °C) or annealing at 300 °C for longer time (240 min) would deteriorate the device performance. The SEM images in Fig. S3 in the ESM show that the Ti/Au contacts have continuous and smooth morphology before annealing, and the Ti/Au contacts remained desirable after optimum annealing at 300 °C in argon for 180 min. However, the contacts degraded significantly with further increase in temperature and time, which led to poor electronic performance.

To further study the electrical contacts at the Ti/β-Ga_2O_3 interface, we conducted TLM measurements in devices with different channel lengths. Figure 3(a) shows an optical image of a typical β-Ga_2O_3 FET with TLM structure. Channel lengths in this TLM structure are measured to be ~ 0.74, ~ 1.04, and ~ 2.74 μm. The fitted total resistance vs. channel length curves in an as-made β-Ga_2O_3 FET measured under different annealing times are shown in Fig. 3(b). Based on the equation $R_{total} = 2 \times R_{contact} + R_{channel}$, the total resistance would be twice as much as the contact resistance when the channel length approaches zero. Thus, $R_{contact}$ can be determined by calculating one half of the y-intercept of the fitted total resistance curves. The contact resistance values in this β-Ga_2O_3 FET at different annealing times were extracted and are summarized in Fig. 3(c). The contact resistance normalized by the channel width decreases from ~ 430 to ~ 0.387 Ω·mm as the annealing time increases to 180 min. Changes in the contact resistance reveal that annealing in argon can effectively improve the device contact resistance and brings $R_{contact}$

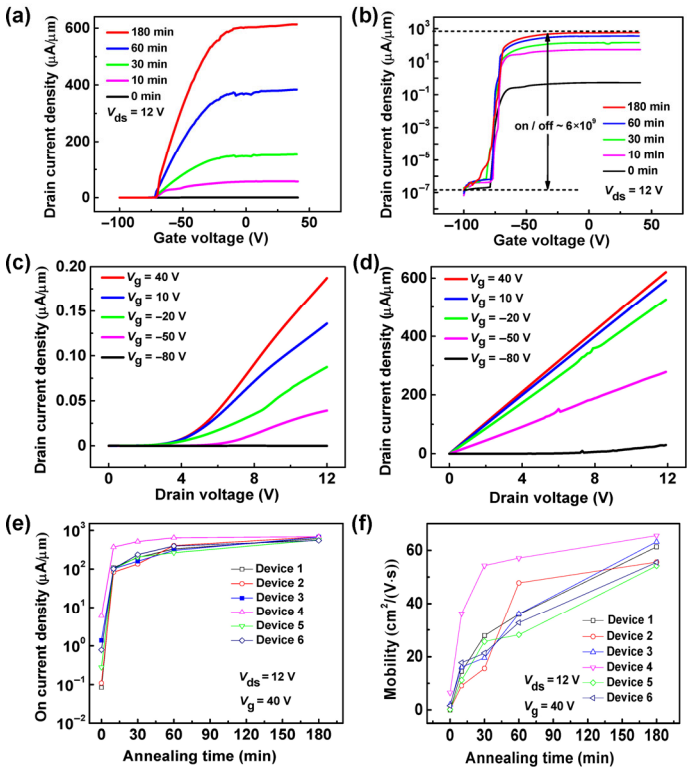

Figure 2 Electronic properties of β-Ga_2O_3 FETs with various annealing times. (a) Typical I_{ds}–V_g curves from a β-Ga_2O_3 FET with various annealing times. (b) I_{ds}–V_g curves from a β-Ga_2O_3 FET shown in logarithmic scale. I_{ds}–V_{ds} family curves from a β-Ga_2O_3 FET at different V_g values (c) before annealing and (d) after annealing. (e) Changes in the on-state current and (f) corresponding field effect mobility changes in the β-Ga_2O_3 FETs at various annealing times for seven devices.

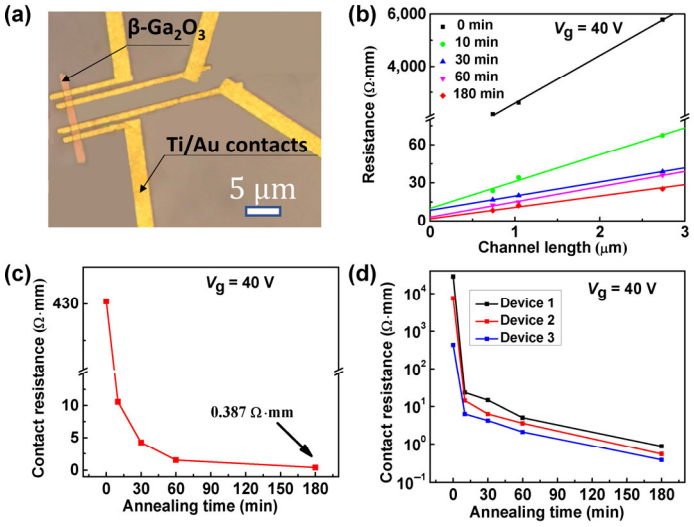

Figure 3 Contact resistance in the β-Ga_2O_3 FETs. (a) Optical image of a β-Ga_2O_3 FET with TLM structure. (b) Total resistance vs. channel length at various annealing times in a β-Ga_2O_3 FET. (c) Contact resistance vs. annealing time in a β-Ga_2O_3 FET. (d) Contact resistance (logarithmic scale) vs. annealing time from three as-made β-Ga_2O_3 FETs with TLM structures.

down to an extremely small level. Figure 3(d) summarizes the improved contact resistance with different annealing times in three β-Ga_2O_3 FETs. Again, one can see that the argon-annealed β-Ga_2O_3 FETs exhibit much lower contact resistance compared to the as-made β-Ga_2O_3 FETs. The results suggest that annealing in argon generally improves the device performance. Reduced contact resistance facilitates electron injection from the metal contacts to the conduction band in β-Ga_2O_3, resulting in low resistance at the metal/semiconductor interface. Such low contact resistance is essential in power electronics. Our results shed light on the importance of annealing, which can be combined with other contact engineering techniques and result in scaled fabrication of high-performance β-Ga_2O_3 FETs.

It is important to understand why annealing causes the observed performance improvements. X-ray spectroscopy (XPS) was employed to examine changes in the material during the annealing process (Fig. S4 in the ESM). Detailed XPS spectra from pure β-Ga_2O_3 and the control samples are shown in Fig. 4. In Fig. 4(a), XPS measurements from pure β-Ga_2O_3 show a major peak at a binding energy of ~ 1,118.0 eV, corresponding to Ga $2p_{3/2}$ in β-Ga_2O_3 [47, 53–55]. The β-Ga_2O_3 3d signal is composed of two separate peaks: one at ~ 20.95 eV binding energy corresponding to Ga $3d_{3/2}$ from β-Ga_2O_3 and another at ~ 20.5 eV corresponding to Ga $3d_{5/2}$ in β-Ga_2O_3 [47, 53–55]. Interestingly, after annealing pure β-Ga_2O_3 in argon at 300 °C for 180 minutes, new peaks with small intensities were observed from XPS measurements. In Fig. 4(b), the new peaks are at lower binding energies compared with the nearby major peaks in pure β-Ga_2O_3. Considering the fact that pure gallium (Ga) materials have a Ga $2p_{3/2}$ peak at 1,116.5 eV and a Ga $3d_{5/2}$ peak at 18.7 eV [55], these new peaks presented in Fig. 4(b) are in the intermediate area between the β-Ga_2O_3 and gallium peaks. These results show that gallium correlates with small oxidation numbers and indicate the existence of oxygen vacancies in β-Ga_2O_3 after annealing in argon [47, 54]. Generating a significant number of oxygen vacancies in β-Ga_2O_3 is difficult, thus they are difficult to detect with XPS in ambient atmosphere [46]. In an oxygen-poor atmosphere like argon, it is much easier to form oxygen vacancies because of their negative formation energy [46]. The pressure from argon atmosphere leads the diffusion of oxygen atoms from normal lattice sites to the gaseous state, generating oxygen vacancies at the surface of β-Ga_2O_3 [44, 47]. These oxygen vacancies would change the chemical states at the surface β-Ga_2O_3 and create new peaks in an XPS spectrum. In Fig. 4(c), similar new peaks can be seen in Ti-coated (1 nm) β-Ga_2O_3, which was annealed in argon at 300 °C for 180 min. Surprisingly, the XPS data from the annealed sample exhibits two shoulders near the major peaks from pure β-Ga_2O_3. Figure 4(c) shows one shoulder near a binding energy of ~ 1,116.6 eV and the other near ~ 19.3 eV. These two shoulders can also be explained by the presence of oxygen vacancies at the Ti/β-Ga_2O_3 interface. There are many Ti_nO_{2n-1} Magnéli phases in the Ti–O system, where Magnéli phases from Ti_2O_3 up to $Ti_{20}O_{39}$ have been discovered [42]. Figure 4(d) shows the free energy of Ti_nO_{2n-1} and β-Ga_2O_3 formation [12, 42]. Figure S5 in the the ESM confirms the existence of a Magnéli phase at the Ti/β-Ga_2O_3 interface after annealing. Since Magnéli phases of a Ti–O system usually have much lower formation energy than β-Ga_2O_3, the Ti metal contacts can easily reduce Ga ions in β-Ga_2O_3 at high temperatures [26–35, 42–48]. Therefore, the two shoulders observed in Fig. 4(c) can be assigned to a high concentration of oxygen vacancies at the Ti/β-Ga_2O_3 interface [47, 53–55]. At high temperature in argon atmosphere, the Ti layer served as a chemically reactive contact to reduce β-Ga_2O_3 and generated a significant number of locally distributed oxygen vacancies at the interface [29, 33, 46–50]. These oxygen vacancies can act as effective electron donors in n-type semiconductors. Thus, "self-doped" surface with oxygen vacancies will narrow the depletion layer, resulting in Ohmic behavior and low contact resistance in electrical contacts on β-Ga_2O_3 FETs.

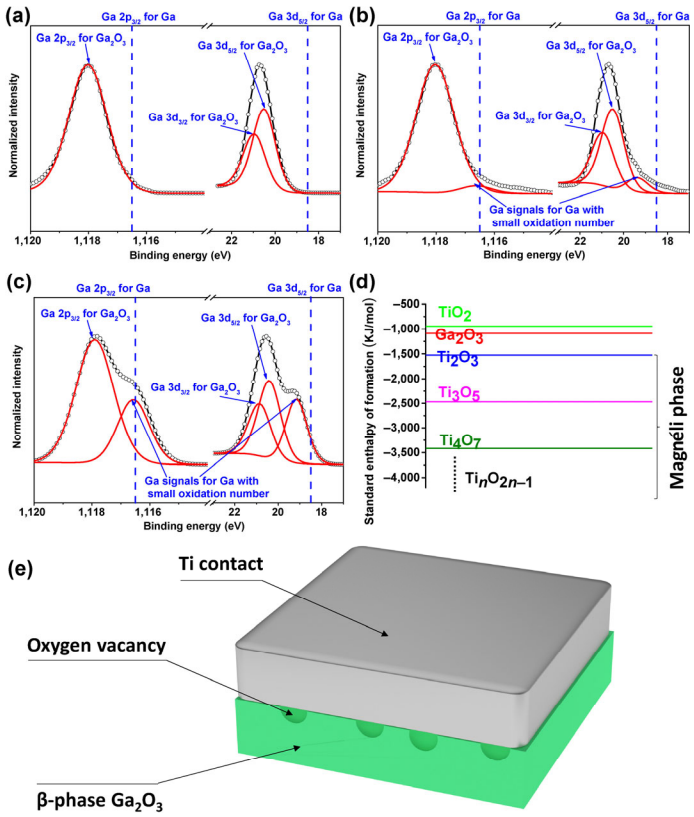

Figure 4 XPS results from β-Ga_2O_3. (a) Normalized Ga $2p_{3/2}$ XPS spectra and Ga 3d XPS spectra from pure β-Ga_2O_3, (b) β-Ga_2O_3 after annealing in argon at 300 °C for 180 min, and (c) Ti-coated (1 nm) β-Ga_2O_3 after annealing in argon at 300 °C for 180 min. Black dots show experimental data red curves show simulated fitting curves. (d) Free energy scheme in different metal oxides. (e) Schematic diagram of the proposed oxygen vacancy model at the Ti/β-Ga_2O_3 interface.

3 Conclusions

In summary, we fabricated β-Ga_2O_3 FETs with Ti/Au contacts and demonstrated that annealing in argon would significantly improve the device performance. The electrical contacts switched from a rectifying behavior to Ohmic behavior at various annealing times. After annealing in argon at 300 °C for 180 min, the β-Ga_2O_3 FETs showed a large saturation drain current density of ~ 3.1 mA/μm and high on/off ratio of ~ 6×10^9. We further showed that the contact resistances reduced to ~ 0.387 Ω·mm after annealing in argon, which can be explained by the generation of oxygen vacancies at the Ti/β-Ga_2O_3 interface. XPS results show that Ti can reduce β-Ga_2O_3 to create a large number of oxygen vacancies, resulted in desirable device contacts. Our results illustrate the important role of metal/β-Ga_2O_3 interfaces in boosting the performance of β-Ga_2O_3 FETs and can further benefit devices made with other metal-oxides and quasi-2D materials

4 Methods

4.1 β-Ga_2O_3 device fabrication and measurements

β-Ga_2O_3 (Sn-doped) was purchased from MTI Corporation. β-Ga_2O_3 was first exfoliated to nanometer scale using vacuum tape (Kapton Tapes). After exfoliation, the sample was dry-transferred onto Si/SiO_2 substrates with alignment markers (SiO_2 thickness of 300 nm), followed by rinsing and residue-removing procedures. A poly(methyl methacrylate) (PMMA) A6 and PMMA A2 bilayer was then spin-coated onto the Si/SiO_2 surface. After spin-coating, electron beam lithography was used to pattern the source/drain electrodes, followed by development, e-beam metal evaporation, and lift-off processes. Ti (10 nm)/Au (150 nm) metal stacks were deposited as

source and drain contacts at 10^{-7} Torr using an e-beam evaporator, and the bottom surface of the silicon substrate served as a global back gate. The electronic properties were measured using an Agilent 4156B semiconductor parameter analyzer. The electron mobility in β-Ga_2O_3 was calculated using the following equation

$$\mu = \frac{L}{W}\frac{1}{C_{ox}V_{ds}}\frac{dI_{ds}}{dV_g} \quad (1)$$

where L and W are the channel length and width in the FET, respectively. I_{ds} is the drain current, V_{ds} is the source-drain voltage, V_g is the gate voltage, and C_{ox} is the gate capacitance per unit area.

4.2 Material characterization

β-Ga_2O_3 materials were examined with AFM (Dimensional, 3100 Digital Instruments, taping mode), Raman spectroscopy (Renishaw Raman with a 532 nm excitation laser and ~ 1 μm laser spot size), XPS (The Kratos Axis Ultra DLD surface analysis instrument using focused monochromatic Al Kα radiation) and TEM (JEOL 2100F, 200KV).

Acknowledgements

We would like to acknowledge the collaboration of this research with King Abdul-Aziz City for Science and Technology (KACST) via The Center of Excellence for Nanotechnologies (CEGN). A portion of the images and data used in this article were acquired at The Center for Electron Microscopy and Microanalysis, University of Southern California.

Electronic Supplementary Material: Supplementary material (Raman spectroscopy of β-Ga_2O_3, air stability performance of β-Ga_2O_3, Ti/Au contacts with different annealing temperature and annealing time, XPS spectra of β-Ga_2O_3, Ti 2p core-level XPS spectra for the Ti-coated (1 nm) β-Ga_2O_3 after annealing, crystal structure of β-Ga_2O_3, SEM images of β-Ga_2O_3 FETs with different metal contacts after annealing, gate leakage current curve at V_{ds} = 12 V, comparison of the device performance of β-Ga_2O_3 FETs) is available in the online version of this article at https://doi.org/10.1007/s12274-018-2193-7.

References

[1] Novoselov, K. S.; Geim, A. K.; Morozov, S. V.; Jiang, D.; Zhang, Y.; Dubonos, S. V.; Grigorieva, I. V.; Firsov, A. A. Electric field effect in atomically thin carbon films. *Science* **2004**, 306, 666–699.

[2] Wang, Q. H.; Kalantar-Zadeh, K.; Kis, A.; Coleman, J. N.; Strano, M. S. Electronics and optoelectronics of two-dimensional transition metal dichalcogenides. *Nat. Nanotechnol.* **2012**, *7*, 699–712.

[3] Carey, B. J.; Ou, J. Z.; Clark, R. M.; Berean, K. J.; Zavabeti, A.; Chesman, A. S. R.; Russo, S. P.; Lau, D. W. M.; Xu, Z. Q.; Bao, Q. L. et al. Corrigendum: Wafer-scale two-dimensional semiconductors from printed oxide skin of liquid metals. *Nat. Commun.* **2017**, *8*, 15116.

[4] Liu, B. L.; Abbas, A.; Zhou, C. W. Two-dimensional semiconductors: From materials preparation to electronic applications. *Adv. Electron. Mater.* **2017**, 3, 1700045.

[5] Kalantar-Zadeh, K.; Ou, J. Z.; Daeneke, T.; Mitchell, A.; Sasaki, T.; Fuhrer, M. S. Two dimensional and layered transition metal oxides. *Appl. Mater. Today* **2016**, *5*, 73–89.

[6] Hwang, W. S.; Verma, A.; Peelaers, H.; Protasenko, V.; Rouvimov, S.; Xing, H. L.; Seabaugh, A.; Haensch, W.; van de Walle, C.; Galazka, Z. et al. High-voltage field effect transistors with wide-bandgap β-Ga_2O_3 nano-membranes. *Appl. Phys. Lett.* **2014**, *104*, 203111.

[7] Higashiwaki, M.; Sasaki, K.; Kamimura, T.; Hoi Wong, M.; Krishnamurthy, D.; Kuramata, A.; Masui, T.; Yamakoshi, S. Depletion-mode Ga_2O_3 metal-oxide-semiconductor field-effect transistors on β-Ga_2O_3 (010) substrates and temperature dependence of their device characteristics. *Appl. Phys. Lett.* **2013**, *103*, 123511.

[8] Irmscher, K.; Galazka, Z.; Pietsch, M.; Uecker, R.; Fornari, R. Electrical properties of β-Ga_2O_3 single crystals grown by the Czochralski method. *J. Appl. Phys.* **2011**, *110*, 063720.

[9] Zhou, H.; Si, M. W; Alghamdi, S.; Qiu, G.; Yang, L. M.; Ye, P. D. High-performance depletion/enhancement-ode β-Ga_2O_3 on insulator (GOOI) field-effect transistors with record drain currents of 600/450 mA/mm. *IEEE Electron Device Lett.* **2017**, *38*, 103–106.

[10] Wu, F. Q.; Chen, L.; Zhang, A. Y.; Hong, Y. L.; Shih, N. Y.; Cho, S. Y.; Drake, G. A.; Fleetham, T.; Cong, S.; Cao, X. et al. High-performance sub-micrometer channel WSe_2 field-effect transistors prepared using a flood–dike printing method. *ACS Nano* **2017**, *11*, 12536–12546.

[11] Galazka, Z.; Uecker, R.; Irmscher, K.; Albrecht, M.; Klimm, D.; Pietsch, M.; Brützam, M.; Bertram, R.; Ganschow, S.; Fornari, R. Czochralski growth and characterization of β-Ga_2O_3 single crystals. *Cryst. Res. Technol.* **2010**, *45*, 1229–1236.

[12] Åhman, J.; Svensson, G.; Albertsson, J. A reinvestigation of β-gallium oxide. *Acta Cryst. Sect C* **1996**, *52*, 1336–1338.

[13] Lovejoy, T. C.; Yitamben, E. N.; Shamir, N.; Morales, J.; Villora, E. G.; Shimamura, K.; Zheng, S.; Ohuchi, F. S.; Olmstead, M. A. Surface morphology and electronic structure of bulk single crystal β-Ga_2O_3 (100). *Appl. Phys. Lett.* **2009**, *94*, 081906.

[14] Ma, N.; Tanen, N.; Verma, A.; Guo, Z.; Luo, T. F.; Xing, H. L.; Jena, D. Intrinsic electron mobility limits in β-Ga_2O_3. *Appl. Phys. Lett.* **2016**, *109*, 212101.

[15] Ramana, C. V.; Rubio, E. J.; Barraza, C. D.; Miranda Gallardo, A.; McPeak, S.; Kotru, S.; Grant, J. T. Chemical bonding, optical constants, and electrical resistivity of sputter-deposited gallium oxide thin films. *J. Appl. Phys.* **2014**, *115*, 043508.

[16] Zhou, H.; Maize, K.; Noh, J.; Shakouri, A.; Ye, P. D. Thermodynamic studies of β-Ga_2O_3 nanomembrane field-effect transistors on a sapphire substrate. *ACS Omega* **2017**, *2*, 7723–7729.

[17] Green, A. J.; Chabak, K. D.; Heller, E. R.; Fitch, R. C.; Baldini, M.; Fiedler, A.; Irmscher, K.; Wagner, G.; Galazka, Z.; Tetlak, S. E. et al. 3.8-MV/cm breakdown strength of MOVPE-grown Sn-doped β-Ga_2O_3MOSFETs. *IEEE Electron Device Lett.* **2016**, *37*, 902–905.

[18] Wong, M. H.; Sasaki, K.; Kuramata, A.; Yamakoshi, S.; Higashiwaki, M. Field-plated Ga_2O_3MOSFETs with a breakdown voltage of over 750 V. *IEEE Electron Device Lett.* **2016**, *37*, 212–215.

[19] Green, A. J.; Chabak, K. D.; Baldini, M.; Moser, N.; Gilbert, R.; Fitch, R. C.; Wagner, G.; Galazka, Z.; McCandless, J.; Crespo, A. et al. β-Ga_2O_3 MOSFETs for radio frequency operation. *IEEE Electron Device Lett.* **2017**, *38*, 790–793.

[20] Chang, P. C.; Fan, Z. Y.; Tseng, W. Y.; Rajagopal, A.; Lu, J. G. β-Ga_2O_3 nanowires: Synthesis, characterization, and p-channel field-effect transistor. *Appl. Phys. Lett.* **2005**, *87*, 222102.

[21] Farzana, E.; Zhang, Z.; Paul, P. K.; Arehart, A. R.; Ringel, S. A. Influence of metal choice on (010) β-Ga_2O_3 Schottky diode properties. *Appl. Phys. Lett.* **2017**, *110*, 202102.

[22] Yao, Y.; Davis, R. F.; Porter, L. M. Investigation of different metals as ohmic contacts to β-Ga_2O_3: Comparison and analysis of electrical behavior, morphology, and other physical properties. *J. Electron. Mater.* **2017**, *46*, 2053–2060.

[23] Ma, Y. Q.; Shen, C. F.; Zhang, A. Y.; Chen, L.; Liu, Y. H.; Chen, J. H.; Liu, Q. Z.; Li, Z.; Amer, M. R.; Nilges, T. et al. Black phosphorus field-effect transistors with work function tunable contacts. *ACS Nano* **2017**, *11*, 7126–7133.

[24] Mann, D.; Javey, A.; Kong, J.; Wang, Q.; Dai, H. J. Ballistic transport in metallic nanotubes with reliable Pd ohmic contacts. *Nano Lett.* **2003**, *3*, 1541–1544.

[25] Ma, Y. Q.; Liu, B. L.; Zhang, A. Y.; Chen, L.; Fathi, M.; Shen, C. F.; Abbas, A. N.; Ge, M. Y.; Mecklenburg, M.; Zhou, C. W. Reversible semiconducting-to-metallic phase transition in chemical vapor deposition grown monolayer WSe_2 and applications for devices. *ACS Nano* **2015**, *9*, 7383–7391.

[26] English, C. D.; Shine, G.; Dorgan, V. E.; Saraswat, K. C.; Pop, E. Improved contacts to MoS_2 transistors by ultra-high vacuum metal deposition. *Nano Lett.* **2016**, *16*, 3824–3830.

[27] Brillson, L. J. Chemical reaction and charge redistribution at metal–semiconductor interfaces. *J. Vac. Sci. Technol.* **1978**, *15*, 1378–1383.

[28] Guo, Y. F.; Zhou, J. Y.; Liu, Y. J.; Zhou, X.; Yao, F. R.; Tan, C. W.; Wu, J. X.; Lin, L.; Liu, K. H.; Liu, Z. F. et al. Chemical intercalation of topological insulator grid nanostructures for high-performance transparent electrodes. *Adv. Mater.* **2017**, *29*, 1703424.

[29] Mosbacker, H. L.; Strzhemechny, Y. M.; White, B. D.; Smith, P. E.; Look, D. C.; Reynolds, D. C.; Litton, C. W.; Brillson, L. J. Role of near-surface states in Ohmic-Schottky conversion of Au contacts to ZnO. *Appl. Phys. Lett.* **2005**, *87*, 012102.
[30] Sawa, A. Resistive switching in transition metal oxides. *Mater. Today* **2008**, *11*, 28–36.
[31] Fortunato, E.; Barquinha, P.; Martins, R. Oxide semiconductor thin-film transistors: A review of recent advances. *Adv. Mater.* **2012**, *24*, 2945–2986.
[32] Waser, R.; Dittmann, R.; Staikov, G.; Szot, K. Redox-based resistive switching memories-nanoionic mechanisms, prospects, and challenges. *Adv. Mater.* **2009**, *21*, 2632–2663.
[33] Yang, J. J.; Strachan, J. P.; Xia, Q. F.; Ohlberg, D. A. A.; Kuekes, P. J.; Kelley, R. D.; Stickle, W. F.; Stewart, D. R.; Medeiros-Ribeiro, G.; Williams, R. S. Diffusion of adhesion layer metals controls nanoscale memristive switching. *Adv. Mater.* **2010**, *22*, 4034–4038.
[34] Yang, J. J.; Pickett, M. D.; Li, X. M.; Ohlberg, D. A. A.; Stewart, D. R.; Williams, R. S. Memristive switching mechanism for metal/oxide/metal nanodevices. *Nat. Nanotechnol.* **2008**, *3*, 429–433.
[35] Gao, X.; Xia, Y. D.; Ji, J. F.; Xu, H. N.; Su, Y.; Li, H. T.; Yang, C. J.; Guo, H. X.; Yin, J.; Liu, Z. G. Effect of top electrode materials on bipolar resistive switching behavior of gallium oxide films. *Appl. Phys. Lett.* **2010**, *97*, 193501.
[36] Javey, A.; Guo, J.; Wang, Q.; Lundstrom, M.; Dai, H. J. Ballistic carbon nanotube field-effect transistors. *Nature* **2003**, *424*, 654–657.
[37] Liu, B. L.; Ma, Y. Q.; Zhang, A. Y.; Chen, L.; Abbas, A. N.; Liu, Y. H.; Shen, C. F.; Wan, H. C.; Zhou, C. W. High-performance WSe_2 field-effect transistors via controlled formation of in-plane heterojunctions. *ACS Nano* **2016**, *10*, 5153–5160.
[38] Mak, K. F.; He, K. L.; Lee, C.; Lee, G. H.; Hone, J.; Heinz, T. F.; Shan, J. Tightly bound trions in monolayer MoS_2. *Nat. Mater.* **2012**, *12*, 207–211.
[39] Wood, J. D.; Wells, S. A.; Jariwala, D.; Chen, K. S.; Cho, E.; Sangwan, V. K.; Liu, X. L.; Lauhon, L. J.; Marks, T. J.; Hersam, M. C. Effective passivation of exfoliated black phosphorus transistors against ambient degradation. *Nano Lett.* **2014**, *14*, 6964–6970.
[40] Desai, S. B.; Seol, G.; Kang, J. S.; Fang, H.; Battaglia, C.; Kapadia, R.; Ager, J. W.; Guo, J.; Javey, A. Strain-induced indirect to direct bandgap transition in multilayer WSe_2. *Nano Lett.* **2014**, *14*, 4592–4597.
[41] Liu, Y.; Guo, J.; Zhu, E. B.; Liao, L.; Lee, S. J.; Ding, M. N.; Shakir, I.; Gambin, V.; Huang, Y.; Duan, X. F. Approaching the Schottky–Mott limit in van der Waals metal–semiconductor junctions. *Nature* **2018**, *557*, 696–700.
[42] Waldner, P.; Eriksson, G. Thermodynamic modelling of the system titanium-oxygen. *Calphad* **1999**, *23*, 189–218.
[43] Yang, J. J.; Strachan, J. P.; Miao, F.; Zhang, M. X.; Pickett, M. D.; Yi, W.; Ohlberg, D. A. A.; Medeiros-Ribeiro, G.; Williams, R. S. Metal/TiO_2 interfaces for memristive switches. *Appl. Phys. A* **2011**, *102*, 785–789.
[44] Lei, B.; Li, C.; Zhang, D.; Tang, T.; Zhou, C. Tuning electronic properties of In_2O_3 nanowires by doping control. *Appl. Phys. A* **2004**, *79*, 439–442.
[45] Liu, Q. Z.; Liu, Y. H.; Wu, F. Q.; Cao, X.; Li, Z.; Alharbi, M.; Abbas, A. N.; Amer, M. R.; Zhou, C. W. Highly sensitive and wearable In_2O_3 nanoribbon transistor biosensors with integrated on-chip gate for glucose monitoring in body fluids. *ACS Nano* **2018**, *12*, 1170–1178.
[46] Hollinger, G.; Skheyta-Kabbani, R.; Gendry, M. Oxides on GaAs and InAs surfaces: An X-ray-photoelectron-spectroscopy study of reference compounds and thin oxide layers. *Phys. Rev. B* **1994**, *49*, 11159–11167.
[47] Dong, L. P.; Jia, R. X.; Xin, B.; Peng, B.; Zhang, Y. M. Effects of oxygen vacancies on the structural and optical properties of β-Ga_2O_3. *Sci. Rep.* **2017**, *7*, 40160.
[48] Varley, J. B.; Weber, J. R.; Janotti, A.; van de Walle, C. G. Oxygen vacancies and donor impurities in β-Ga_2O_3. *Appl. Phys. Lett.* **2010**, *97*, 142106.
[49] Carey IV, P. H.; Yang, J. C.; Ren, F.; Hays, D. C.; Pearton, S. J.; Jang, S.; Kuramata, A.; Kravchenko, I. I. Ohmic contacts on n-type β-Ga_2O_3 using AZO/Ti/Au. *AIP Adv.* **2017**, *7*, 095313.
[50] Carey IV, P. H.; Yang, J. C.; Ren, F.; Hays, D. C.; Pearton, S. J.; Kuramata, A.; Kravchenko, I. I. Improvement of Ohmic contacts on Ga_2O_3 through use of ITO-interlayers. *J. Vac. Sci. Technol. B* **2017**, *35*, 061201.
[51] Qian, Y. P.; Guo, D. Y.; Chu, X. L.; Shi, H. Z.; Zhu, W. K.; Wang, K.; Huang, X. K.; Wang, H. et al. Mg-doped p-type β-Ga_2O_3 thin film for solar-blind ultraviolet photodetector. *Mater. Lett.* **2017**, *209*, 558–561.
[52] Strachan, J. P.; Pickett, M. D.; Yang, J. J.; Aloni, S.; David, K. A. L.; Medeiros-Ribeiro, G.; Stanley Williams, R. Direct identification of the conducting channels in a functioning memristive device. *Adv. Mater.* **2010**, *22*, 3573–3577.
[53] Zhao, Y. Y.; Frost, R. L. Raman spectroscopy and characterisation of α-gallium oxyhydroxide and β-gallium oxide nanorods. *J. Raman Spectrosc.* **2008**, *39*, 1494–1501.
[54] Bourque, J. L.; Biesinger, M. C.; Baines, K. M. Chemical state determination of molecular gallium compounds using XPS. *Dalton Trans.* **2016**, *45*, 7678–7696.
[55] Naumkin, A. V.; Kraut-Vass, A.; Gaarenstroom, S. W.; Powell, C. J. NIST X-ray photoelectron spectroscopy database, NIST standard reference database 20, version 4.1. Gaithersburg MD: National Institute of Standards and Technology, 2000.